ORIGINAL RESEARCH ARTICLE

Acoustic Emission Sensor-Assisted Process Monitoring of Air Plasma-Sprayed Titanium Deposition

V. Viswanathan[1] · Anil Prathuru[2] · Nadimul Haque Faisal[2] · Saurav Goel[1,3]

Abstract Acoustic emission is a sensing technique that offers the potential benefit for its use as an in situ monitoring tool for a wide range of manufacturing processes. This work attempts to highlight the robustness of using acoustic emission (AE) data for in-line process monitoring of the air plasma spray deposition technique. As part of this study, titanium powder was deposited under various conditions of robot speed, powder feed rates and the influence of these changes were investigated in the signature obtained from the AE analysis. The post-processed AE data showed sensitivity to these changes through variation in frequencies, power spectral densities and the cumulative energy that gets transmitted to the substrate during the spraying process. The AE signal sensitivity was found to be so robust that it picked up even the differences in the substrate conditions i.e., a substrate used for coating in an as received form vs a substrate that was grit blasted before spraying showed identifiable differences in the AE signature. An attempt to convert an AE signal to energy and then analyse the spraying process in light of the cumulative energy is an investigation first of its kind in this research, hitherto not seen in the literature. In light of the extensive experimental data gathered from the in-house deposition data, the influence of the release of elastic strain energy based on the particle states and the impact on the substrate has been discussed thoroughly. The interdependency of surface preparation, feed rate and the robotic gun scanning speed has been discussed in detail as well. Through the data presented in this study, we advocate the use of AE analysis to be a vital contributor and a welcome move towards digitalisation of the thermal spray process for in-process monitoring.

Introduction

The thermal spray process is expected to be a market worth USD 25.82 billion by 2027, and the powders used in thermal spraying involve several critical raw materials that are vital for the working of a useful range of components including turbine blades, cutting tools, medical implants and food rolls to list a few. The real-time monitoring and diagnosis of the thermal spray process become tediously challenging, given the rapidity of the process, which is the major reason why the thermal spray sector has not benefitted from digitalisation methods and tools. The process continues to be stirred manually by trying out variations in the process parameters based on trials-and-errors. Hence, there is a considerable incentive to further understand the spraying process through the eyes of robust sensing tools.

Controlling the variables and process parameters (Ref 1) during thermal spraying can be critical to obtaining desired coating properties since the deposition process is circumscribed by a range of simultaneously occurring complex phenomena ranging from plasma state of matter, high velocity physics, shock induced crystallisation, residual stress formation, heating and cooling gradients in the

✉ Anil Prathuru
a.prathuru@rgu.ac.uk

1 School of Engineering, London South Bank University, 103 Borough Road, London SE1 0AA, UK

2 School of Engineering, Robert Gordon University, Garthdee Road, Aberdeen AB10 7GJ, UK

3 Department of Mechanical Engineering, University of Petroleum and Energy Studies, Dehradun 248007, India

materials and hot erosion and wear. Capturing all the complex processes occurring at complex lengths and time scales will be a distant vision for a thermal spray enthusiast, however, the process can well be studied by discretising it into small problems. For instance, the temporal evolution of overall coating formation constitutes individual splat formation, flattening to form deposition layers followed by cooling to room temperature followed by materials recrystallisation and bonding with the substrate. The process is well influenced by the use of gas, particle size distribution, in-flight particle behaviour characterised by variations in temperature and velocity, substrate geometry, nozzle geometry, spray gun characteristics, powder feed rates and gas flow rates, etc. This inherent data-dependent nature of the thermal spray process lends itself to be highly amenable to a process optimisation. In addition, the use of spray monitoring sensors and process control systems can lead to the production of high volumes of data which can be used to create process maps with input and output inter-relational characteristics. Thus, there is an opportunity to apply instrumentation and measurement methods to the thermal spray process in a robust manner and study the process in detail.

Acoustic emission (AE), which is defined as transient elastic stress waves produced by a release of energy from a localized source, is a sensing technique that tends to recognise the acoustic signature of a process. This can be in the amplitude-time domain as well as the more advanced amplitude-frequency-time domain. Traditionally, AE has been used reliably for manufacturing processes (apart from many other applications) which do not involve extreme heat gradients at the base of the substrate such as machining, drilling and cutting (Ref 2-4).

The first use of AE to examine post-thermal-sprayed coating part dates to the mid-1990s (Ref 5-7) when efforts were made to understand the coating adhesion. Tillman et al. (Ref 8) performed in situ monitoring of thermal spray using AE. They employed a filtering method that separates the spray noise from the recorded signal leaving behind the material response signature. With these considerations, they demonstrated the crack formation during coating deposition, as well as delamination through the use of acoustic emission signatures in the energy spectrum. A quantitative relation was shown between the material response signature and the coatings' physical structure (crack network density, porosity). Faisal et al (Ref 9) monitored HVOF thermal spray using AE sensors. An attempt was made at reducing the particle impacts by spraying through slits. The recorded signal cumulative energy is correlated to the spray spot area through the slits. The use of AE in particle impact monitoring has led to the quantification of erosion wear during metal and glass particle impact (Ref 10). This investigation on the low

velocity (2.5-7.1 m/s) impact of brass and glass particles on metal plates showed that the AE signal can reliably identify the degree of plastic deformation induced by the particle impact. The authors calculated the transfer functions of the plate to deconvolute the source signal. In addition, they were also able to estimate the particle size based on the impact force. Taniguchi et al. (Ref 11) introduced the use of laser-based AE detectors (non-contacting) to monitor post-sprayed coating. In their study, four laser sensors were focussed on the substrate and the relative arrival times of the signal arising due to cracking were used to locate the crack location. Calculated arrival times in conjunction with finite element analysis of the coating thermal state-induced interfacial stresses were used to predict the critical maximum principal stress of the coating failure. No significant signal analysis was done on the AE records. The purpose of AE was to estimate the crack initiation time with respect to specimen temperature. Wang et al. (Ref 12) utilised AE in the crack propagation monitoring of TBCs under a uniaxial tension load. Based on the observed tensile load behaviour and AE records, they suggested that the crack initiation and initial propagation are associated with low frequency AE, whereas crack propagation leading to final failure emits high frequency AE. As before, this study used AE on post-sprayed failure evaluation of coatings.

The use of AE as a diagnostic tool has been implemented in some studies for particle sizing in impact conditions. Hu et al (Ref 13) implemented a smoothed local energy-based peak picking algorithm that can identify individual particle impacts. The accuracy of the proposed algorithm was tested at different particle flow rates. It was shown that as the flow rate increases, the overlap between individual particle impacts increases as well, which can lead to the misidentification of events. While the algorithm was shown to be very accurate with larger particles due to the high amplitude produced, the signal produced by smaller particles was shown to be comparable to the noise due to air flow. Similar behaviour is expected with thermal spray where a wide range of impinging molten particles are expected to flow at high velocities of about 700-900 m/s.

Kamnis et al. (Ref 14) used multiple diagnostic methods (particle velocimetry, spray plume aero-acoustics) in diagnosing particle flow in thermal spray. The recorded frequencies of the spray plume noise have been correlated with the coating properties using neural networks. The use of Hertzian contact mechanics in modelling the impact force and produced force pulse has been proposed by a few studies (Ref 15, 16). The peak impact force is proportional to the density, radius, and velocity of the particle.

The elastic strain energy transferred to the substrate due to the particle kinetic energy in thermal spray leads to elastic pressure wave propagation within the substrate. A

key hypothesis can thus be formed that the wave propagation in the substrate due to the particle strike can reveal information about the governing mechanisms of the coating formation to learn further about the extent of the elastic and plastic deformation occurring during thermal spraying. This knowledge is critical in better understanding the coating evolution to perform real-time diagnosis or to detect anomalies such as inconsistencies in the substrate surface condition.

Thus, the current study explores the use of AE to monitor the particle impact during the air plasma spray (APS) variant of the thermal spray process taking titanium powder as a testbed. The effect of particle flow rate, gun speed and substrate conditions were explored, and the related acoustic emission data analysed to establish the frequency response of different spray conditions was examined.

Experimental Procedure

Air Plasma Spraying

A thermal spray setup with 6 Axis robot (supplied by ABB,UK, S4C controller Serial Number: 24-12758,) mounted with Metco, Westbury USA made F4MB-XL Plasma spray gun, was used for studying the particle impact induced AE. A commercially available powder of pure Titanium (Metco 4012A) was deposited on a low carbon steel (Grade 1006-1026) substrate of dimension 600 mm × 300 mm × 2 mm with Argon gas since these combinations are routinely used in spray industries and thus, the novel findings from this study will directly be transferrable. The reported particle size of the powder is 45 μm to 150 μm (Fig. 1b). Figure 1(a) shows the morphology of the titanium powder captured through scanning electron microscopy in secondary electron mode. Particle size distribution was calculated through ImageJ software and is shown in Fig. 1(b). The details of the process parameters used to perform the thermal spray during this work are shown in Table 1. This meant that the location of the spray line changed between the different experiments. However, it did not make any difference in the captured AE signals.

Acoustic Emission Instrumentation

In all the experimental trials, the location of the sensor was at least 40 mm (shortest distance) away from the spray path. To ensure avoiding damage to the piezoelectric material of the AE emission sensor, it was necessary to mount the sensor on the base plate safely. The substrate temperature for the various spray parameters and combinations of geometries used in this work was monitored through a thermal imaging camera from FLIR USA (Model No. T540) to ensure that the temperature did not go past a threshold limit that could damage the sensor. An overall scheme of the AE sensor assembly and instrumentation is shown in Fig. 2.

The sensors used were the physical acoustics corporation (PAC) Micro-80D broadband sensors supplied by Mistras Group Ltd, UK. The frequency response band of these sensors lies between 175 and 900 kHz. It is to be noted that the sensor is capable of detecting frequencies lower than 100 kHz; however, the signal amplitude response in these frequencies is much lower compared to that in the response band. Part of the Modal analysis performed on the plate under the given boundary conditions
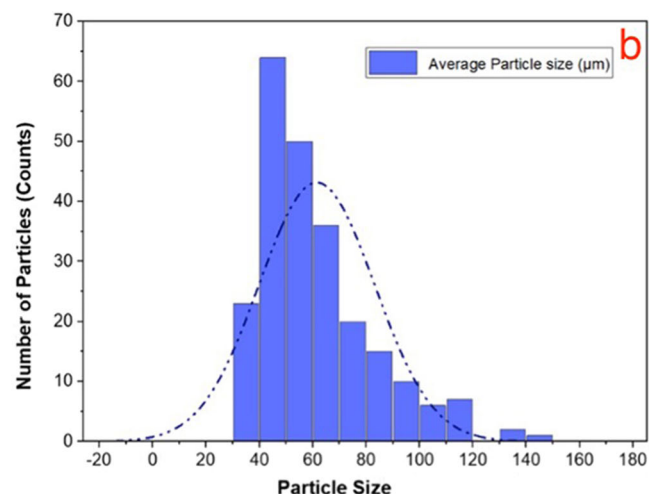

Fig. 1. (a) Titanium powder (Metco 4012A) observed through a scanning electron microscope for understanding the morphology and, (b) the size range

Table 1. Process parameters used in this study for titanium deposition and its monitoring using acoustic emission

Gun current	550 Amps
Voltage supplied to the gun	18 V
Primary gas (Argon)	3 m³/h Argon @ 9.65 bar
Spray Distance (mm)	100 mm
Carrier Gas (argon)	0.48 m³/h carrier
Hopper pressure	4.13 bar
Blasting	Grit blasted using garnets of 24 grit (680 μm) size

Fig. 2. Spray data acquisition layout
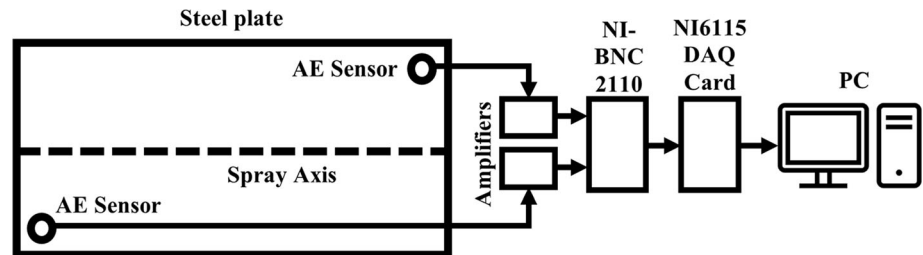
revealed that the natural frequencies of the plate are well below the detectable threshold of the sensor and so will not appear in the sensor data records. This meant that the data acquired by the sensors is purely due to the particle and gas interactions with the plate. The AE sensors were connected to physical acoustics corporation supplied 2/4/6 preamplifiers with a chosen amplification level of 20 dB. These pre-amplifiers were in turn connected to a BNC 2110 block which collects the data streams and transmits the data to the computer through a PCI-6115 data acquisition card (DAQ). LabVIEW software was used to create a visual interface to set the data acquisition parameters for the spray experiments and to store the sensor generated data. The amplifiers, BNC block, DAQ and the software were all supplied by National Instruments (NI) Ltd, UK. In all the experiments, a data acquisition rate (or sampling rate) of 2 MHz was used. The sensors were mounted onto the substrate using high temperature silicone grease and aluminium adhesive tape to achieve proper sealing for excellent data acquisition. The location of the sensors was chosen such that there was enough heat dissipation along the signal propagation path ensuring that the operation of the sensors is not affected. However, the location also means that the propagation of the signal through the plate displays dispersion meaning that the particle impact source signal frequency response is modified by the plate properties over long propagation time and distance.

Experimental Methodology

Before the use of AE during spraying, some static offline tests were performed to ensure the working of the AE setup. This was done through the standard pencil lead break

(PLB) test which is also called as Hsu-Nielsen source following the name of the inventors of this test (Ref [14]). Five equidistant points were marked on the plate along the length on the centre axis, indicated by the dashed line in Fig. 2. This centre line also depicts the initial spray path of the plasma spray gun. Five PLBs were conducted on each point and the data was averaged. These tests confirmed the frequency response of the plate which is specific to its geometry and material properties. As the aim of the study is focussed on the classification of the AE characteristics of individual components of plasma spray, the initial trials involved rastering the gun on the substrate just with the plasma flow as this aid to capture the AE signature of powderless flow (only plasma) on the plate. The effect of the gun speed was also studied with the gun raster speed increased from 0.5 to 0.8 m/s. The experiment was repeated with this higher speed and just the plasma flow.

In the next set of experiments, the powder flow rate was set to 5 g/min to establish the AE characteristics of particle impacts. This value is lower than the typical value used in a production setting. This was chosen to better establish the AE characteristic frequency of powder impacts without overwhelming the sensor. It is well known that grit blasting the substrate aids the mechanical bonding of the coating during the thermal spraying process. Two substrate surface conditions (as received—no grit blasting, grit blasted) were compared through experimentation with the same parameters as above and AE signals were recorded in both cases. Establishing the AE characteristic of this case was thought to help establish the distinction between successful coating formation and particle rebound. To this end, initial experiments with a 5 g/min powder flow rate were carried out with a substrate with no surface grit blasting. Three repetitions of this experiment were carried out with 0.5 and

0.8 m/s gun speed. The powder flow rate was increased to 15 g/min to understand the AE signature of higher particle impact numbers at the stated gun speeds and surface conditions. The same experiments were then repeated with a grit blasted substrate. The set of experiments performed in this study is summarised in Table 2. The last column of this table indicates the outputs of the coating process. Y indicates coating formation and N indicates that either a coating did not form, or it did not adhere (peel off) to the substrate.

In addition to these, experiments with the sensors mounted on the substrate with the spray jet directed away from it were conducted to establish the background noise of the spray booth. The results corresponding to all these experiments are presented in the next sections.

AE Data Analysis

The cumulative energy (E) during an AE event is calculated as the area under the absolute voltage (V) signal with respect to time (t), given by (1).

$$E = \int |V(t)| dt \qquad \text{(Eq 1)}$$

An attempt to convert an AE signal to energy and then analysing the spraying process in light of the cumulative energy is an attempt first of its kind in this study, hitherto not seen in the literature in the context of thermal spray. Cumulative energy has also been calculated for the signals collected with the different spray conditions and used to distinguish between the powder flow rate and substrate surface conditions. An attempt was made to characterise the frequency response of the particle impact at different spray parameters. Semi-log power spectral density (PSD) plots are used to distinguish and identify the frequency windows that can characterise the varying impact response.

The signal associated with these frequency windows was then quantified using energy calculations to estimate the overall energy distributions and changes in this with the process parameter change. In addition, the significant peaks associated with these frequency windows were identified and the changes in these were tracked with the changing process parameters. This led to the identification of powder flow related frequency characteristics.

Results and Discussion

AE Signals and Dispersion Curves

This section presents the data analysis carried out on the signal records acquired during thermal spraying using the acoustic emission sensor. Though two sensors were used, the results presented correspond to the sensor mounted on the top right of the substrate's back face. This is because of the significant overlap of the single particle events given the aggregate number of particles impacting the substrate every second. In such circumstances, the use of multiple sensors to locate individual event locations turned out to be close to impossible, thus negating the significance of using multiple sensors.

The wave dispersion response of the steel substrate was first characterised by estimating the group velocity dispersion curves shown in Fig. 3. As seen, the plate exhibits three significant wave modes within the measurable frequency range with the used AE sensor as confirmed using the Hsu-Nielsen pencil lead break (PLB) tests. This test involves breaking a 0.5 mm diameter 2H grade pencil on the substrate and recording its AE signal. The PLB was used to simulate a point source of AE, like the one produced by particle impacts.

Table 2. Spray conditions tested with the AE sensor mounted on the substrate

Experimental condition	Powder flow rate, g/m	Substrate condition	Gun traverse speed, m/s	Number of passes	Coating deposition (Y/N)
1	0	As received	0.5	3	N
2	0	As received	0.8	3	N
3	5	As received	0.5	3	N
4	5	As received	0.8	3	N
5	5	Grit blasted	0.5	3	Y
6	5	Grit blasted	0.8	3	Y
7	15	As received	0.5	3	Y
8	15	As received	0.8	3	Y
9	15	Grit blasted	0.5	3	Y
10	15	Grit blasted	0.8	3	Y

Fig. 3. Dispersion curves of 2 mm thick steel plate within the frequency range of 0-1 MHz
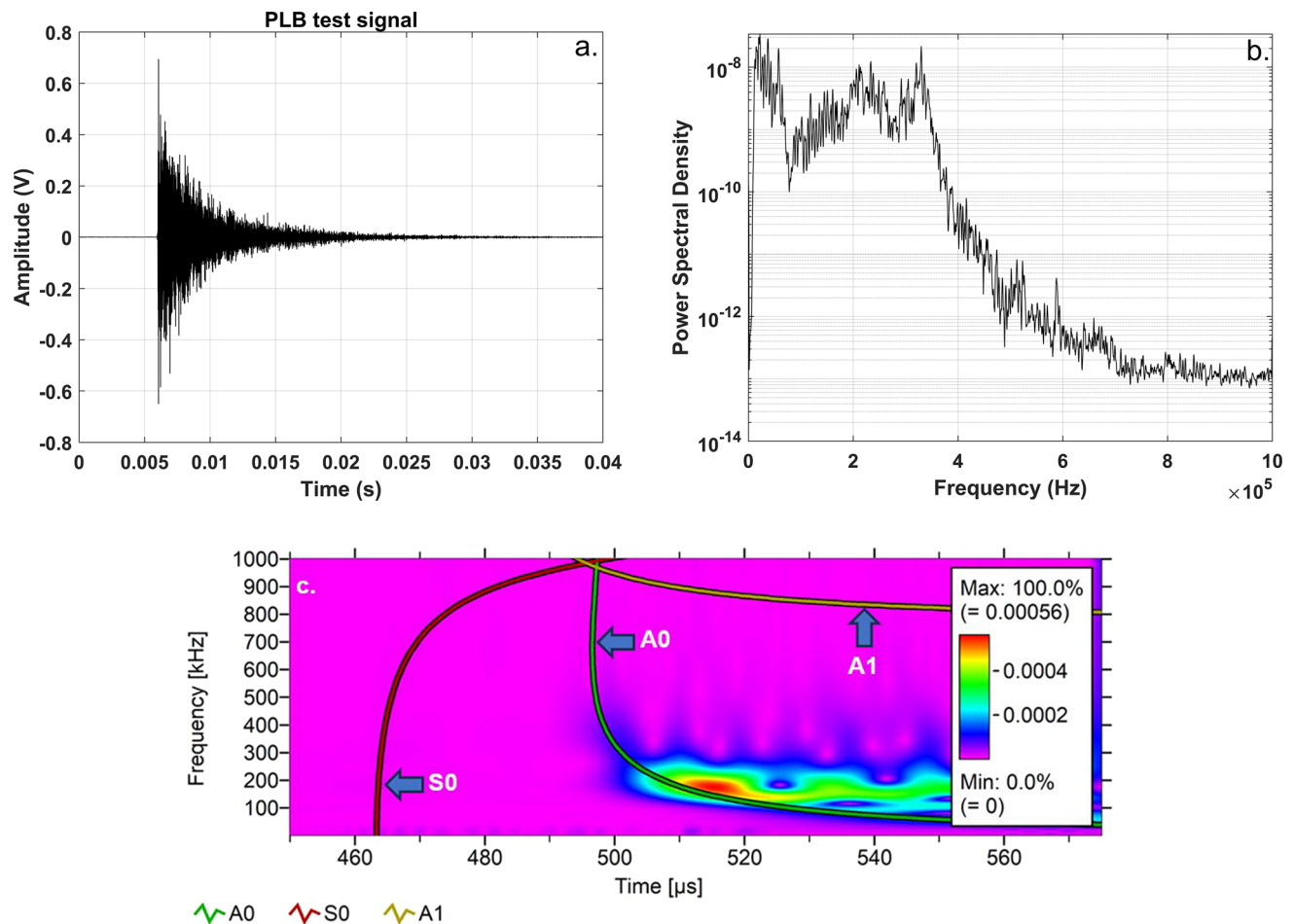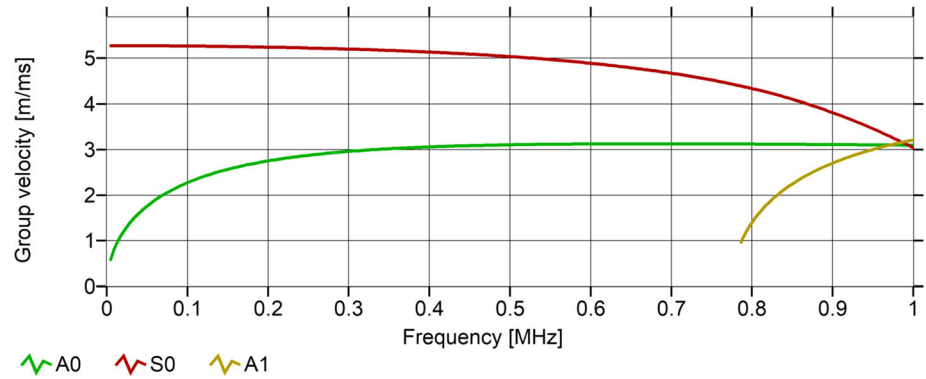

Fig. 4. (a) Time domain signal, and (b) semi-log power spectral density plot of PLB test conducted on the substrate (c) wavelet transform of the AE record of a PLB test carried out at a distance of 250 mm from the sensor location. Prominent wave modes are shown

Figure 4 shows the amplitude (Fig. 4a) and frequency response (Fig. 4b) of the substrate under a simulated AE event. The high response in the lower frequencies is to be noted, especially under 100 kHz. There is little to no response in the frequencies above 600 kHz and so is not shown in the plot.

Prosser et al. (Ref 15) demonstrated that the significant wave mode in a metal plate due to low velocity impact is fundamental flexural (A0), whereas the fundamental extensional component (S0) dominates in the high velocity regime. The A0 component is induced by the normal impact of particles where the induced shear deformation

within the substrate is insignificant, whereas the S0 component is induced due to the shear and lateral displacement of the substrate at higher particle velocities at room temperature. The particle size in the current study is considerably smaller than that employed by Prosser et al (Ref 15). In addition, melting is also expected in the particles, which meant that the impact conditions are of molten droplets on a solid, rigid body. Given this and the observed frequency response, it is postulated that the plasma spray particle impact induced AE activity within the substrate is principally due to the fundamental flexural mode (A0) propagation. The close-to-molten state of the particles is not expected to induce high shear deformation within the substrate. This is apparent from Fig. 4(c) which shows the wavelet transform (WT) for a PLB test conducted at 250 mm from the sensor. This is attributed to the impact of particles to the substrate. The dispersion curves for a 2 mm thick steel plates have been superimposed on to the WT plot, which show that except for the fundamental A0 mode, two other wave modes are of negligible magnitudes.

Gas and Powder Flow Pointed Away from the Substrate

To establish the AE signature of the gas flow through the plasma spray gun and circulation around the spray booth, initial experiments were conducted with the gun pointed away from the substrate at 100 mm, this distance is measured from the right edge of the substrate to the exit of the nozzle parallel to the longest edge of the substrate. The sensor positions were studied separately both on the substrate and on the gun. The signal from the AE sensor was recorded in these conditions. Figure 5(a) shows a sample signal record and the corresponding frequency spectrum of the signal is shown in Fig. 5(c). From Fig. 5(c) and (d), it can be inferred that the major component of the signal falls within low frequencies. This is noteworthy despite the low sensitivity of the used sensors at frequencies below 100 kHz. It can also be seen from Fig. 5(c) and (d) that the presence of powder in the gas flow does not affect the frequency spectrum in this case as the gun is pointed away from the substrate. This analysis showed the major component of the signal energy lies in frequency ranges lower than 100 kHz.

Analysis done this way, indicated significant activity in the 0-100 kHz frequency range. Thus it can be concluded that this frequency response corresponds to the plate vibrations induced by the gas flow within the chamber and so can be used to isolate the powder impact induced frequency response. This was seen to be the case with all the experiments conducted.

Gas and Powder Flow on the Substrate

Influence of Powder Flow

To establish the influence of powder flow, the gun was raster scanned on the plate at a traverse speed of 0.5 m/s with gas flow, without powder flow and with powder flow. The corresponding results are shown in Fig. 6. The frequency response of the first case (plasma only) was very similar to the case with the gun pointed away from the substrate. This shows that the plasma flow directly onto the substrate does not introduce any additional/different wave propagation within the plate and the dominant vibrations are of low frequency and high amplitude. Next, titanium powder was introduced into the flow at 2 flow rates i.e., 5 and 15 g/min. The two values are to allow the understanding of changes in signal characteristics, if any, with changes in the powder flow rate. As shown in Fig. 6(b) and (c), the introduction of powder particles into the plasma stream does change the signal characteristic evidenced by the considerable increase in the frequency response above 300 kHz. As soon as the spray plume spot initiates contact with the substrate, the frequency response changed with activity seen all over the monitored frequency spectrum. Activity is seen to increase dramatically in the 300 kHz-1 MHz range. This is attributed to the impact of particles to the substrate. This remains consistent with both the tested powder flow rates, though the number of particles with the latter is expected to be substantially higher leading to a 'densely packed' impact generated signal pattern. Regardless, the frequency response characterised by the significant peaks with both these powder flow rates is nearly identical. To better understand these frequency responses, four zones are marked in each plot in Fig. 6, based on the observed peaks within the recorded spectrum. The introduction of powder does not significantly make any difference in Zone I, except for a decrease in the PSD in cases where the powder flow rate is non-zero. However, it enhances the frequency response significantly in Zone 'III' and 'IV'. These observations indicate that the higher frequencies can be used as an indicator of the powder flow on to the substrate. It is to be noted that the surface condition of the substrate was as-received with no grit blasting for these experiments. Interestingly, with all the experimental conditions, the frequency response of the signal did not change with time and across multiple passes. This is understandable given the low number of passes and low coating thickness build-up. This means that the addition of the coating layers is not enough to significantly change the wave mode dispersion behaviour of the substrate. With higher coating thickness build up however,
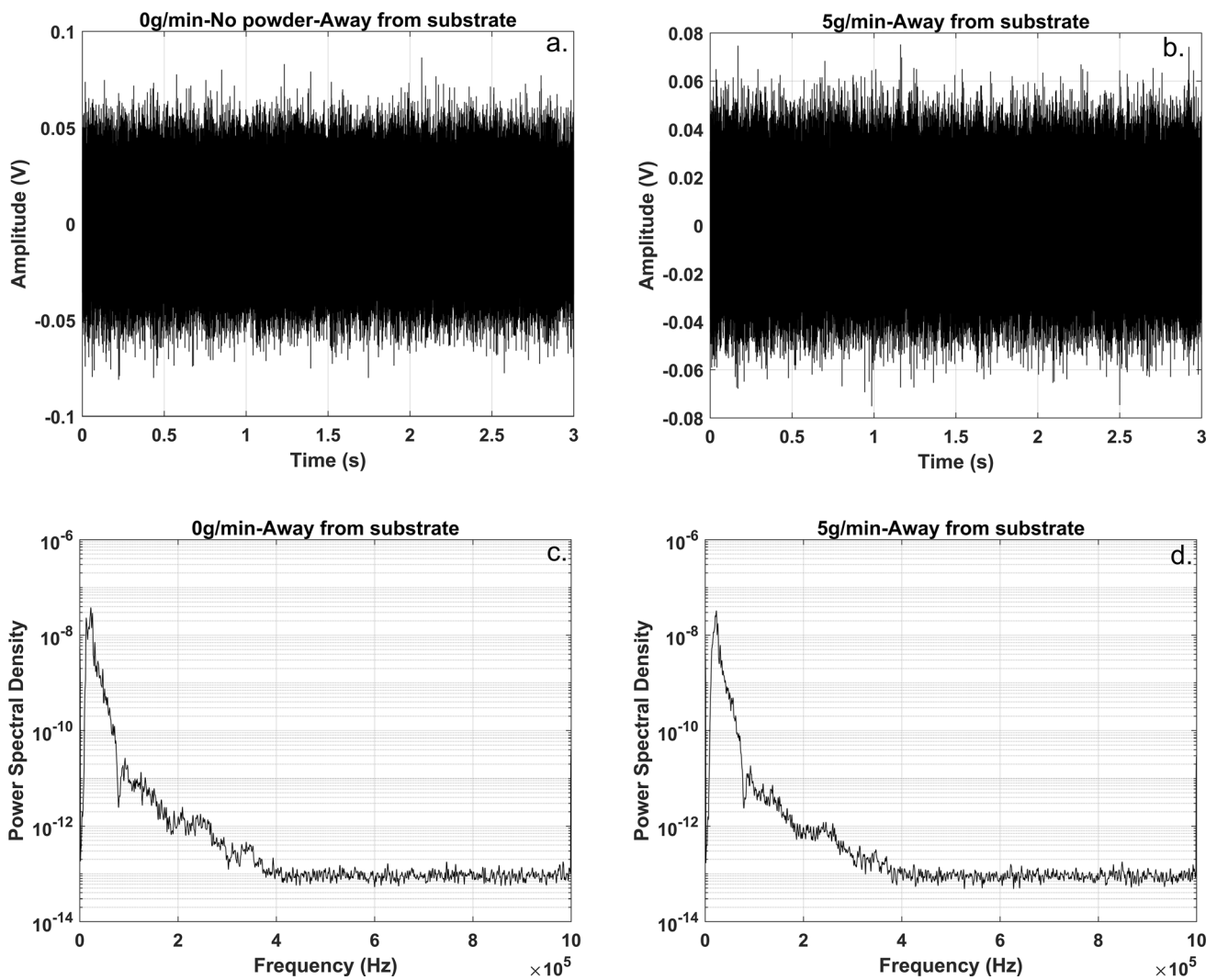
Fig. 5. Voltage vs time signals (a) without and (b) with powder, power spectral density (c) without and (d) with powder, spray gun pointed away from the substrate

development of residual stresses across multiple layers due to quenching might lead to microcracking which will register as major events in the AE response of the coating process. For this to be recorded, future work will need to conduct experiments with higher number of passes.

Given that no surface preparation was applied to the substrate, very little to no coating formation was expected with these spray conditions. This was the case with the 5 g/min powder flow rate. With the higher flow (15 g/min), patches of thin coating layers were noticed. It is also to be noted that each experiment had three passes of the gun over the substrate. The energy associated with these frequency windows was plotted as a function of the powder flow rate in Fig. 7(a). This plot quantifies the energy variations at different frequencies with the changing powder flow rate. Figure 7(a) highlights that the energy plots were mapped across three frequency ranges (100 kHz-low-pass, 300-500 kHz bandpass and 500 kHz-high-pass). The case

where there was no powder flow was taken to be the base case and the two other powder flow rate cases were normalised against this. Normalisation was done for individual frequency bands. It may be seen that the increasing powder flow rate increases the normalised energy within each band. A significant increase in the energy can be seen from 5 to 15 g/min compared to 0-5 g/min. It is to be noted that a thin layer of coating formation was observed with a 15 g/min flow rate even without any surface preparation. It is also interesting to see that the 100 kHz-low-pass energy does not exhibit significant changes with the introduction of powder, though a slight reduction is seen in this frequency band with the highest powder flow rate, further strengthening the observation that the powder impact response lies in the higher frequency bands.

Another measure of the powder flow rate could be the AE signal energy that can be calculated in situ during the spraying process. At higher powder flow rates, given the
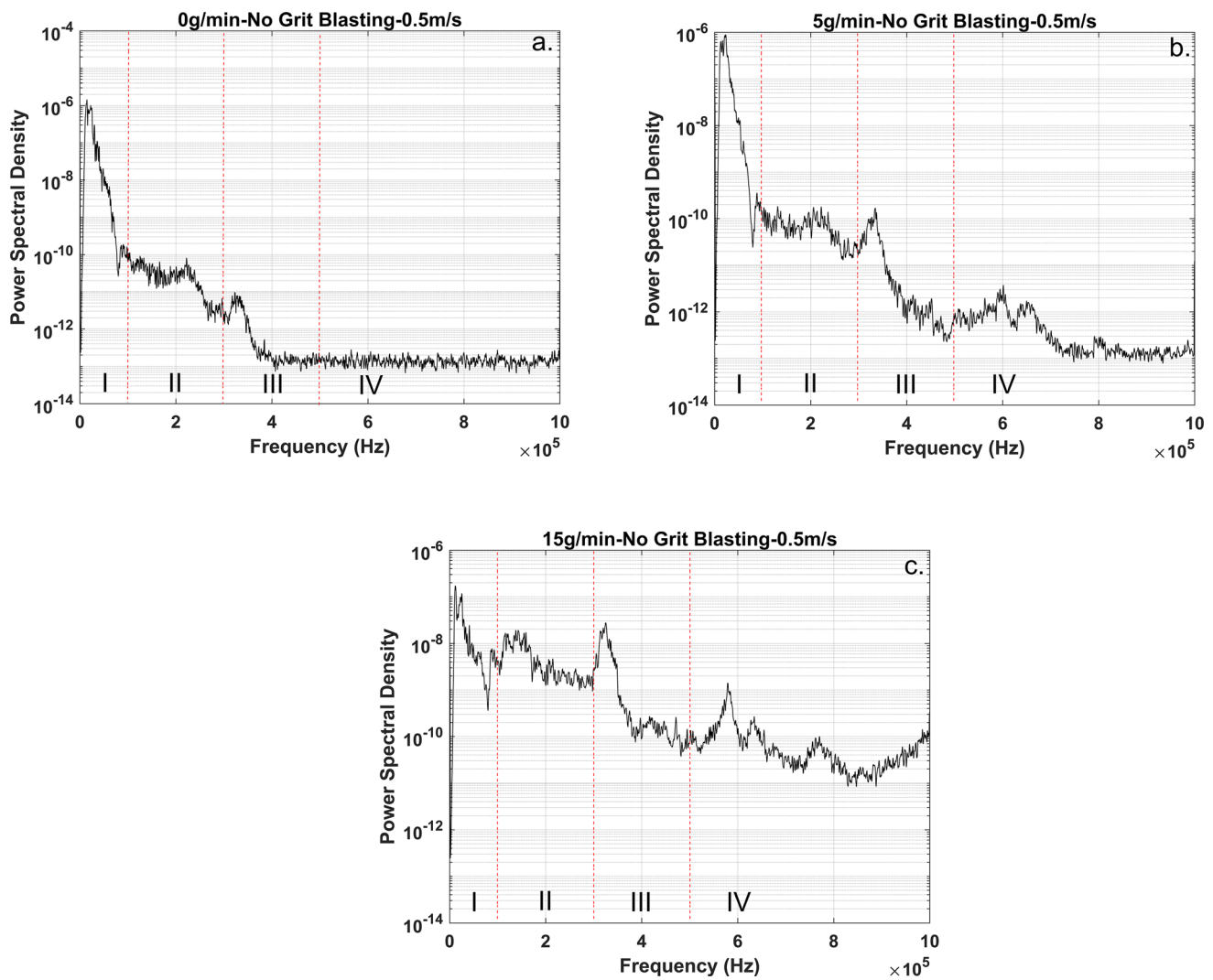
Fig. 6. Semi-logarithmic power spectral density plots of AE signals recorded with (a) no powder flow, (b) powder flow of 5 g/min, and (c) powder flow of 15 g/min and a spray gun raster speed of 0.5 m/s

higher number of particles hitting the surface, the net AE energy per unit record time is bound to be higher. This phenomenon is shown in Fig. 7(b). As seen the gradient of the cumulative energy curve against time is larger with the higher powder flow rate. Considering Fig. 7(a), the higher gradient is due to the higher energy content in the > 300 kHz frequency band.

Influence of Gun Traverse Speed

To understand the effect of increasing the gun raster speed across the substrate, the same powder flow conditions were used with a gun speed of 0.8 m/s. The frequency band energy content plots for the three powder flow conditions (0, 5, 15 g/min) are shown in Fig. 8(a). As shown, these are very similar to those seen in Fig. 7(a). Given the faster gun speed, the number of particles impacting the substrate

surface is expected to be lower. This explains the lower power spectral density and cumulative energy values seen in Fig. 8(a) and (b) compared to Fig. 7(a) and (b) respectively. No compounding effects of raster speed combined with powder flow rate were observed, meaning that the effects of raster speed and powder flow rate were independent of each other.

Influence of Surface Preparation

The third set of results attempts to understand the capability of the AE technique in distinguishing the surface condition of the substrate and subsequent influence on the coating formation/adhesion with the substrate during plasma spray. To this end, the same powder flow rates as before were used, this time with a grit blasted surface to induce surface adhesion. The semi-logarithmic plots of the
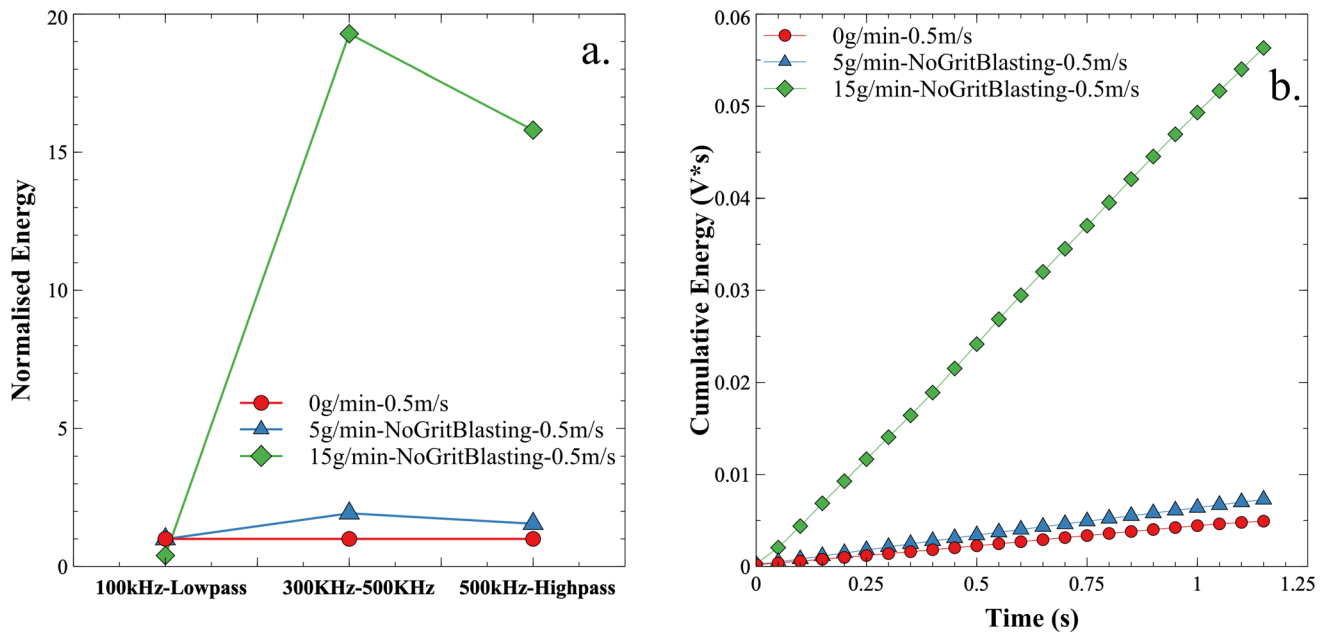
Fig. 7. (a) Variation in the normalised energy levels at 0.5 m/s robot speeds at different frequency bands with 5 g/min and 15 g/min powder flow rates, (b) Cumulative energy variation with the powder flow rate at gun raster speed of 0.5 m/s
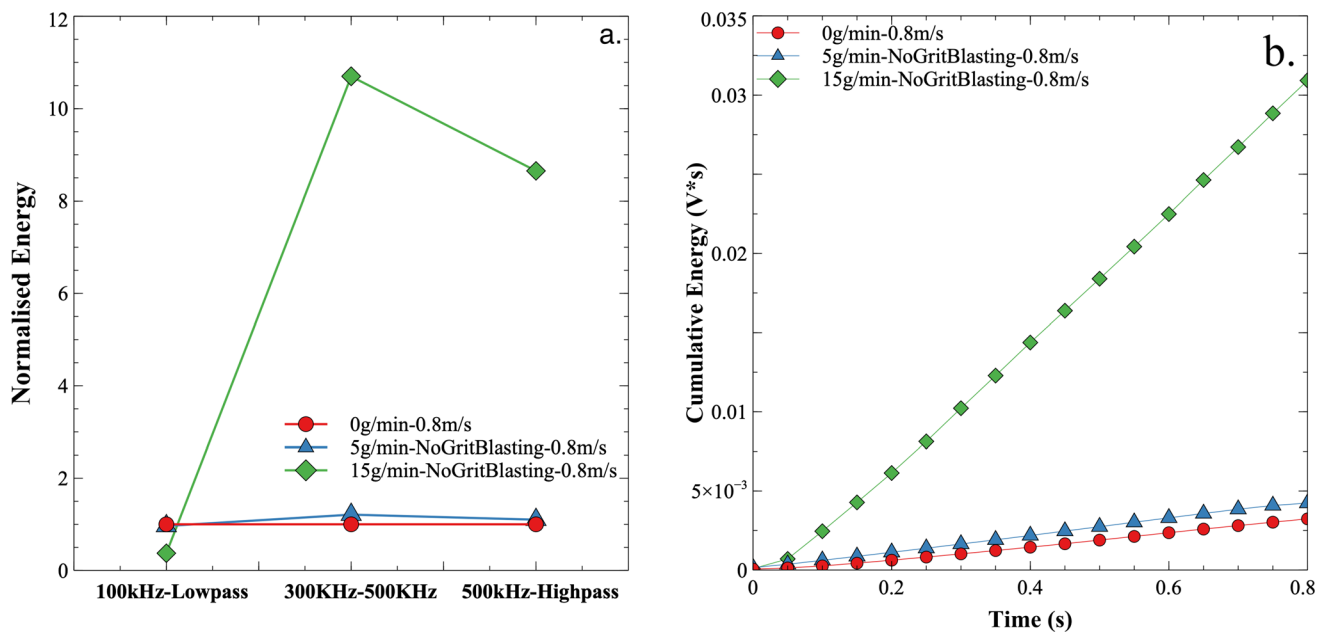

Fig. 8. (a) Variation in the normalised energy levels at 0.8 m/s robot speeds at different frequency bands with 5 g/min and 15 g/min powder flow rates, (b) Cumulative energy variation with the powder flow rate at gun raster speed of 0.8 m/s

power spectral density of the different flow rates are shown in Fig. 9. As before, four frequency bands were identified in the frequency band between 0 and 1 MHz.

Compared to the plots presented before in Fig. 6(b) and (c), the plots shown in Fig. 9(a) and (b) show significant changes in the frequency-energy response. This is more apparent with a 15 g/min powder flow rate (Fig. 9b). There is also a noticeable shift in the frequency peaks in zones II

and IV. Comparing Fig. 6(c) and Fig. 9(a), the frequency peaks and the energy distribution exhibit similar characteristics. It is also to be noted that in both these cases, there was a similar coating thickness formation. In other words, creating a better bonding surface through grit blasting created a similar effect as increasing the powder flow rate with an untreated surface. This is reflected in the frequency response of the coating formation process. With the higher
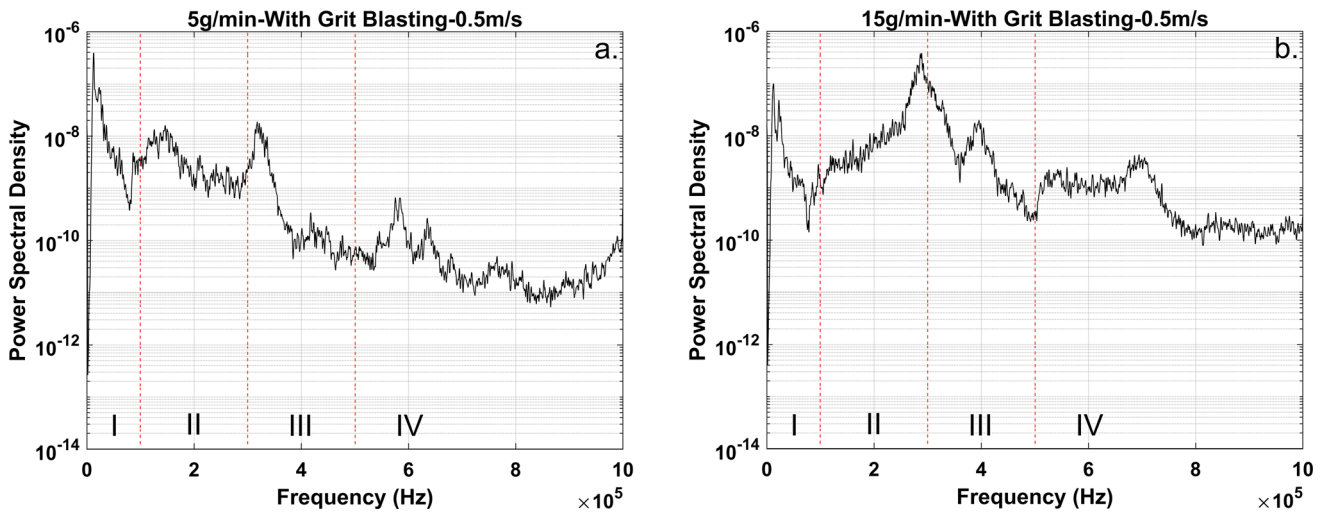
Fig. 9. Power spectral density plot for grit blasted substrates with (a) 5 g/min, and (b) 15 g/min powder flow rates with 0.5 m/s raster speed
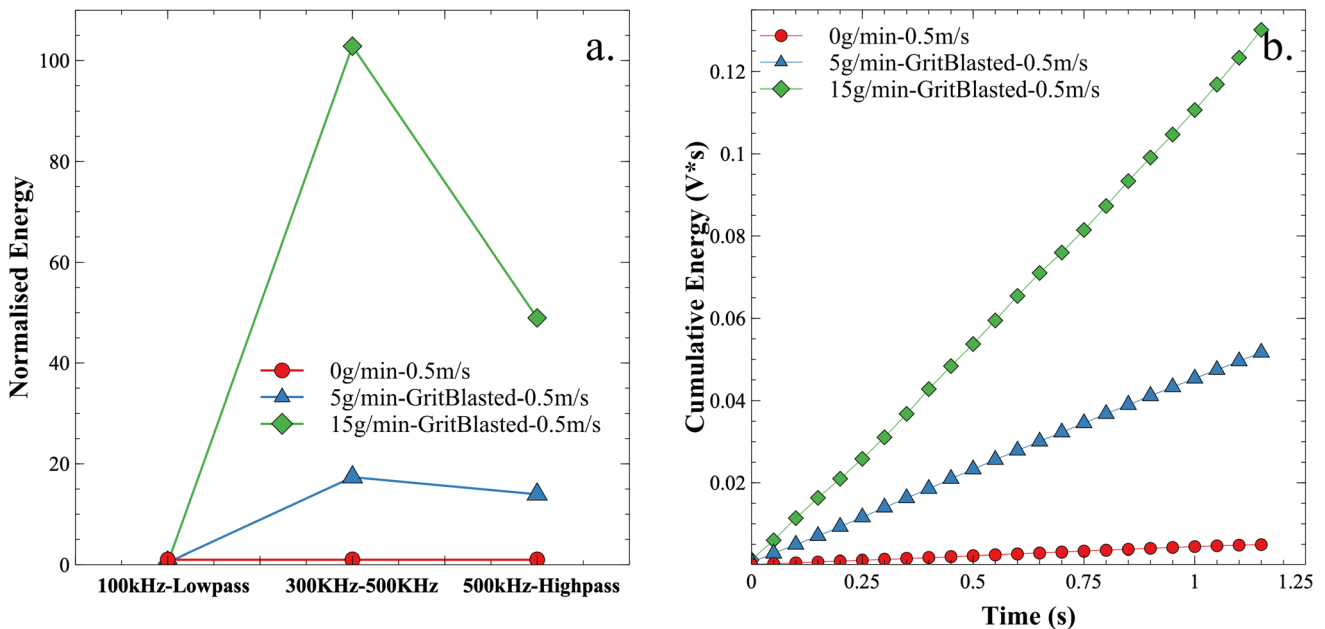

Fig. 10. (a) Normalised energy content of the different frequency bands with different powder flow rates and grit blasted substrate surface, (b) cumulative energy content of the AE signal records, with different powder flow rates and grit blasted substrate surface

powder flow rate and with a grit blasted surface, coating formation of higher thicknesses was observed, though not high enough to significantly impact the wave dispersion behaviour of the substrate. Thus, this shift in the frequency response can be seen as an indicator of coating formation. In addition to the above three frequency bands, a significant increase in the response was also seen in the 100-300 kHz frequency band. It is to be noted that the resonant frequency of the sensor used in this investigation is 305 kHz. The observed frequency response is expected to differ with a different sensor. To compensate for this,

sensors that have broadband flat frequency response are recommended for use in industrial settings.

Figure 10(a) indicates the variation in the energy distribution within the frequency bands shown in Fig. 9. The energy ratios of the different frequency bands appear to be similar for the case with 5 g/min powder flow rate on a grit blasted surface from Fig. 10(a) and 15 g/min powder flow rate on the substrate with no grit blasting from Fig. 7(a). The energy content of the 100 kHz-low-pass band is seen to be quite similar across the different powder flow rates used. The increase in the high frequency content with the highest powder flow rate was larger showing high energy

transfer to the substrate from the incoming particles. Given the coating formation with this condition, it can be postulated that the net kinetic energy transfer to the substrate is significantly enhanced by the adhesion of the particles to the substrate. Given that the utilised powder material is Titanium, no significant cracking is expected within the coating layers upon cooling. Hence, it can be said that the AE record energy is primarily from the particle impact.

With a 15 g/min powder flow rate, surface preparation almost doubles the cumulative energy captured by the substrate because more powder particles can adhere to a grit blasted substrate thereby enabling better deposition efficiency and thickness development. In general, grit blasted surfaces (Fig. 10b) showed at least twice the cumulative energy compared to their non grit blasted counterparts (Fig. 7b).

Further Analysis and Critical Discussions

For a 5 g/min powder flow rate with an average titanium particle size of 70 microns, the expected particle rate per micro-second is roughly 1 particle hitting the substrate. This seems to correspond to the period between two corresponding signal peaks seen in the signal records. To understand the particle impact induced signal amplitude, the gas flow induced frequencies as seen in Fig. 5(c) and (d) have been filtered out using a 100 kHz-high-pass filter. After this, it was seen that the signal amplitude is small at the lower powder flow rate. With a higher powder flow rate of 15 g/min, the average number of particles rate per microsecond is 3. It is not clear if these particles create overlapping wavelets and if the overlap will be constructive or destructive.

Figure 11 shows the peak frequency and the corresponding PSD values for different frequency bands for the different specimens. From Fig. 11, it can be seen that the peak frequency within the < 100 kHz frequency band shifts to around 12 kHz in conditions where coating formation was observed. It is possible that the particle impact also contributes to the low frequency spectrum. However, as this is common with the gas flow, the differentiating factor is seen to be the high frequency content. A raster speed of 0.5 m/s was seen to have higher high frequency energy compared to 0.8 m/s (Fig. 12). Higher raster speed was expected to have a lower number of particle impacts on the substrate due to the lower amount of time taken to traverse the width of the substrate corresponding to a lower amount of residence time of the gun on the substrate. Regardless of the observed frequency response and energy content of the signal, the number of particles impacted by the different raster speeds is the same. With the grit blasted substrate and powder flow rate of 15 g/min, the signal shows a gradient in the initial stage where the spray spot
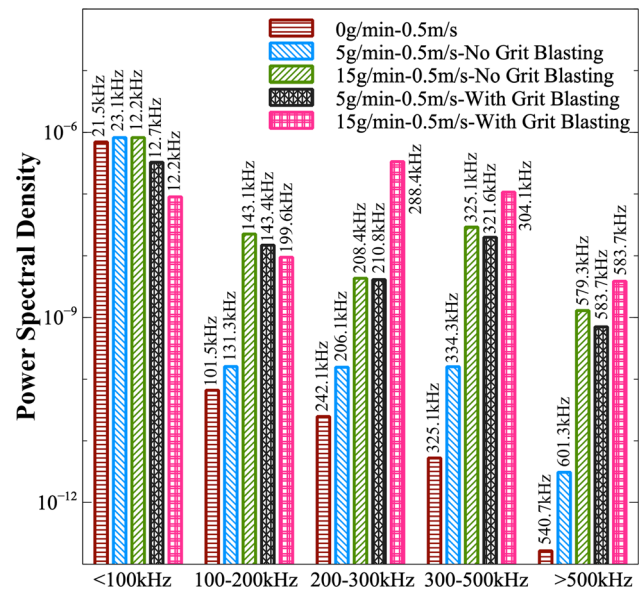

Fig. 11. Normalised power spectral density (PSD) of AE signals seen in high and low powder feed rates and with/without surface grit blasting
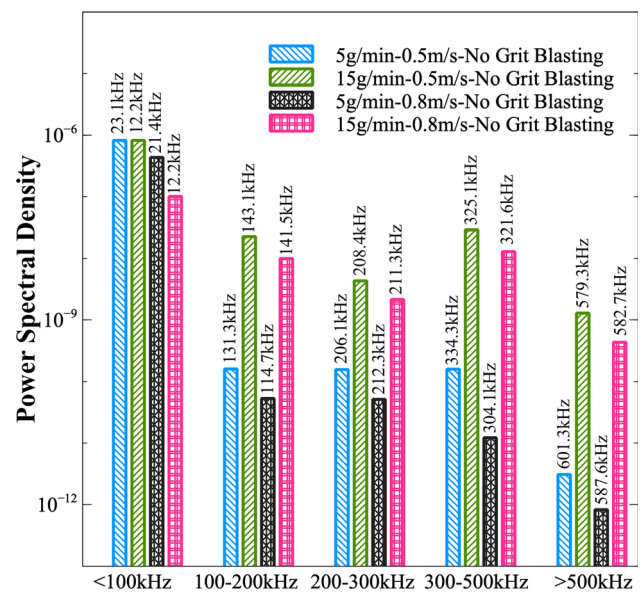

Fig. 12. Normalised power spectral density (PSD) of AE signals seen in experiments with high and low powder feed rates, high and low robot speed and with/without grit blasting

(circular) gradually comes into contact with the substrate. This also implies a gradient in the number of particles hitting the substrate, increasing from zero to the maximum. The amplitude of the signal shows a gradual increase in this stage. Frequency analysis of the signal shows that the response is consistent throughout implying that the frequency response is dependent on the particle impact induced coating deposition rate. With the maximum powder flow rate on the grit blasted substrate, the frequency

spectrum shows a dominant peak of 288 kHz, which is close to the resonant frequency of the sensor (Fig. 11).

The shift in the frequency peaks with a 15 g/min powder flow rate on the grit blasted substrate could have been due to the increased bonding rate of the particles with the better surface condition amenable to bonding. The particle impact phenomenon is characterised by an exchange of energy between the particle and the substrate. The impacting particle has more thermal and kinetic energies. Depending on the ratio of these two, the coating formation is either kinetic energy related plastic deformation driven, or thermal energy related melting/softening driven. In either case, a portion of the kinetic energy and the induced strain rate becomes responsible for the splat formation of the particle. The rest of the kinetic energy is transferred to the substrate as an impact force, the magnitude of which is determined by the particle degree of deformation related to the incoming velocity. The particle impact time is a function of the particle elastic-plastic properties, and particle velocity. The kinetic energy transferred to the substrate during impact is also determined by the degree of plastic deformation within the particle at low velocities (Ref 16, 17). This transferred force causes local plastic deformation in the substrate around the impact zone and being transferred to the substrate, is also responsible for some degree of elastic deformation. The energy associated with this is stored as elastic strain energy within the substrate and is consequently transferred to the particle in the rebound phenomenon. If the rebound energy is higher than the bond energy between the particle and substrate, the particle rebounds and the strain energy is transferred to the particle leading to the particle accelerating away from the substrate. In the case of good bonding, this rebound strain energy will not be able to break the bond between the particle and substrate and the rebound strain energy stays within the particle-substrate system. Moreover, after the deposition of the coating layers, the medium for the elastic wave propagation changes and is now thicker leading to lower energy dissipation in the boundaries. It is to be noted that the elastic deformation is responsible for the acoustic emission response of the particle impact and in the latter case with coating bonding, a higher AE response is expected due to the trapping of the elastic rebound energy within the substrate. This is reflected in the higher amplitude in higher powder flow rates and better bonding conditions as shown in Fig. 13.

Previous studies reported that the fraction of kinetic energy responsible for AE is around 3% to 7% for particle velocities of around 70 m/s at room temperature (Ref 15). Despite the higher particle velocity, due to the higher particle temperature and resulting melting, this fraction might be lower in the case of plasma spray. Moreover, if the particles have undergone extensive melting, the AE
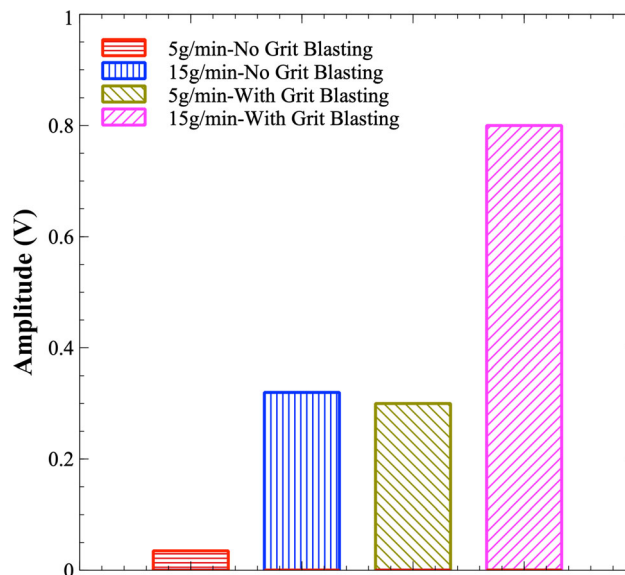

Fig. 13. Variation of the AE record peak amplitude with powder flow rate and substrate surface condition

produced would be due to the elastic impact of liquid droplets rather than solid. In this case, the AE production could partially be due to the reflection of pressure waves within the liquid droplet. With liquid droplets impacting on ceramic substrates, the amplitude of the AE event produced was shown to be directly proportional to the impact kinetic energy (Ref 18). Moreover, previous studies on the use acoustic emission method in process monitoring applications such as particle impact employed some form of signal classification algorithms such as K-means, nearest neighbour, etc., to estimate different particle sizes and impact velocities. In such studies, the number of particles impacting the substrate was relatively low with little to no overlap between the AE signal produced by subsequent particle impacts. This meant that individual particle impacts could be isolated and analysed for signal characteristics for subsequent classification. In the current case however, subsequent particle impacts produced significant overlaps which meant that isolating individual events and AE characteristic extraction was not possible. Hence, the signal analysis had to rely on fundamental amplitude and frequency analysis to understand the influence of the spray parameters.

From the perspective of subsequent particle impacts and consequent AE signal characteristics, a probable explanation could be given for the observed frequencies with the different experimental conditions. Given the powder mass flow rate of 5 g/min, particle density and size, it was estimated that around 100,000 particles hit the substrate every second which translates to a time interval of 10 microseconds assuming consecutive particle impacts. However, there may be a significant overlap between the

impact events at any time point which will add to the constructive or destructive interference of the generated pressure waves within the material. At higher powder flow rates, i.e., 15 g/min, the number of particles hitting the substrate is 3 times higher than the case of using a mass flow rate of 5 g/min and the time interval between consecutive particle impacts reduces. Considering two subsequent particle impacts, if the frequency of the wave generated by the first particle impact is such that its period matches the time to the next particle impact, constructive interference occurs between the two generated waves creating a standing wave within the plate upon successive impacts. This condition will also be satisfied for integer multiples of the base frequency. Thus, these peaks may appear in the frequency spectrum of the particle impact AE record. It is to be kept in mind that plate wave propagation exhibits dispersion meaning that as the wave propagates within the plate, the energy will be spread across multiple frequencies. Also, boundary condition dependent edge reflections further distort the waves within the plate. However, constructive interference occurs only at certain frequencies, dependent on the periods, assuming consecutive particle impact. Thus, further in-depth signal analysis aided by numerical simulations of particle impact induced wave propagation could be beneficial. Also, further work can be directed to delineate the AE wave propagation for different coating microstructural patterns. Porosity, unmelts, and surface interface cleanliness could be quantified with AE thereby reducing metallography requirements in manufacturing.

Conclusions

The feasibility of using AE for in-line process monitoring of the thermal spray process was accessed through an indigenous experimental plan involving experimental trials of atmospheric plasma spray of titanium powder on the steel substrate with a robot mounted air plasma spray gun. This attempt to perform this sensing in real-time was novel considering the high surface temperatures emerging from the plasma conditions of the spray. For purposes of the experiments, two opposite (adverse and amendable) conditions were considered. An attempt to convert an AE signal to energy and then analysis the spraying process in light of the cumulative energy is an attempt first of its kind in this study. Based on the experimental outcomes, the following conclusions can be drawn:

a. The AE method can reliably sense the differences in the mass flow rate of the powder, vis-à-vis sensing the change of cumulative AE energy as a function of time. This was seen to be a net result of the cumulative effect of the AE impact events produced due to the particle impacts.

b. AE signal showed good sensitivity to the change in the substrate surface conditions and powder flow rates which appears to follow a specific pattern in terms of the frequency band. For instance, the frequencies > 500 kHz signified a good mass flow rate of the powder, whereas low frequencies of < 100 kHz indicated the footprint of plasma alone without any powder. Overall, most frequency bands obtained from this study indicated that the events during thermal spray can be consolidated in three frequency bands of < 300 kHz, 300 kHz-500 kHz and > 500 kHz. Activity in these frequency bands was significantly higher than in the no-powder condition leading to quantification of these parameters.

c. The frequency response of the acquired signals with and without surface preparation demonstrated a large difference attributed to the behaviour of the substrate-coating system in signal transmission.

Data Availability The data produced in this work will be made available upon reasonable request.

References

1. V. Venkatachalapathy, N.K. Katiyar, A. Matthews, J.L. Endrino, S. Goel, A Guiding Framework for Process Parameter Optimisation of Thermal Spraying, Coatings, 2023.

2. B. Zhou, H. Ye, H. Zhang and M. Li, Process Monitoring of Iron-Making Process in a Blast Furnace with PCA-Based Methods, *Control. Eng. Pract.*, 2016, **47**, p 1–14.

3. C.A. My, C.H. Le, M. Packianather and E.L.J. Bohez, Novel Robot Arm Design and Implementation for Hot Forging Press Automation, *Int. J. Prod. Res.*, 2019, **57**(14), p 4579–4593.

4. D. Dornfeld, Application of Acoustic Emission Techniques in Manufacturing, *NDT & E Int.*, 1992, **25**(6), p 259–269.
5. C.K. Lin, S.H. Leigh and C.C. Berndt, Acoustic Emission Responses of Plasma-Sprayed Alumina-3% Titania Deposits, *Thin Solid Films*, 1997, **310**(1-2), p 108–114. https://doi.org/10.1016/S0040-6090(97)00366-0
6. J. Voyer, F. Gitzhofer and M.I. Boulos, Study of the Performance of TBC under Thermal Cycling Conditions using an Acoustic Emission Rig, *J. Therm. Spray Technol.*, 1998, **7**(2), p 181–190. https://doi.org/10.1361/105996398770350909
7. C.C. Berndt, C.K. Lin and S.H. Leigh, Characterization of Cracking within Thermal Spray Deposits by an Acoustic Emission Method, *J. Therm. Spray Technol.*, 1998, **7**(3), p 334–336. https://doi.org/10.1361/105996398770350800
8. W. Tillmann, F. Walther, W. Luo, M. Haack, J. Nellesen and M. Knyazeva, In Situ Acoustic Monitoring of Thermal Spray Process Using High-Frequency Impulse Measurements, *J. Therm. Spray Technol.*, 2018, **27**(1), p 50–58.
9. N.H. Faisal, R. Ahmed, R.L. Reuben and B. Allcock, AE Monitoring and Analysis of HVOF Thermal Spraying Process, *J. Therm. Spray Technol.*, 2011, **20**(5), p 1071–1084.
10. D. Buttle and C. Scruby, Characterization of Particle Impact by Quantitative Acoustic Emission, *Wear*, 1990, **137**(1), p 63–90.
11. K. Taniguchi, M. Enoki, M. Watanabe, S. Kuroda and K. Ito, In situ monitoring of cracking behaviors of plasma-sprayed coatings by the laser acoustic emission technique, *J. Mater. Res.*, 2009, **24**(10), p 3182–3189.
12. L. Wang, C.G. Liu, X.H. Zhong, Y.X. Zhao, H.Y. Zhao, J.S. Yang, S.Y. Tao and Y. Wang, Investigation of Crack Propagation Behavior of Atmospheric Plasma-Sprayed Thermal Barrier Coatings under Uniaxial Tension Using the Acoustic Emission Technique, *J. Therm. Spray Technol.*, 2015, **24**(3), p 296–308.
13. Y. Hu, X. Huang, X. Qian, L. Gao and Y. Yan, Online Particle Size Measurement Through Acoustic Emission Detection and Signal Analysis, 2014 IEEE International Instrumentation and Measurement Technology Conference (I2MTC) Proceedings, IEEE, 2014, p 949–953.
14. S. Kamnis, K. Malamousi, A. Marrs, B. Allcock and K. Delibasis, Aeroacoustics and Artificial Neural Network Modeling of Airborne Acoustic Emissions During High Kinetic Energy Thermal Spraying, *J. Therm. Spray Technol.*, 2019, **28**(5), p 946–962.
15. J. Ukpai, R. Barker, X. Hu and A. Neville, Determination of Particle Impacts and Impact Energy in the Erosion of X65 Carbon Steel Using Acoustic Emission Technique, *Tribol. Int.*, 2013, **65**, p 161–170.
16. C. Pecorari, Characterizing Particle Flow by Acoustic Emission, *J. Nondestruct. Eval.*, 2013, **32**(1), p 104–111.
17. N.N. Hsu and F.R. Breckenridge, Characterization and Calibration of Acoustic Emission Sensors, *Mater. Eval.*, 1981, **39**(1), p 60–68.
18. W.H. Prosser, M.R. Gorman and D.H. Humes, Acoustic Emission Signals in Thin Plates Produced by Impact Damage, *J. Acous. Emiss.*, 1999, **17**(1-2).